

This work was written as part of one of the author's official duties as an Employee of the United States Government and is therefore a work of the United States Government. In accordance with 17 U.S.C. 105, no copyright protection is available for such works under U.S. Law.

Public Domain Mark 1.0

<https://creativecommons.org/publicdomain/mark/1.0/>

Access to this work was provided by the University of Maryland, Baltimore County (UMBC) ScholarWorks@UMBC digital repository on the Maryland Shared Open Access (MD-SOAR) platform.

Please provide feedback

Please support the ScholarWorks@UMBC repository by emailing scholarworks-group@umbc.edu and telling us what having access to this work means to you and why it's important to you. Thank you.

RESEARCH ARTICLE | MAY 08 2006

Transport and fluctuations in high temperature spheromak plasmas^{a)}

H. S. McLean; R. D. Wood; B. I. Cohen; E. B. Hooper; D. N. Hill; J. M. Moller; C. Romero-Talamas; S. Woodruff



Phys. Plasmas 13, 056105 (2006)

<https://doi.org/10.1063/1.2192469>



CrossMark

Transport and fluctuations in high temperature spheromak plasmas^{a)}

H. S. McLean,^{b)} R. D. Wood, B. I. Cohen, E. B. Hooper, D. N. Hill, J. M. Moller, C. Romero-Talamas, and S. Woodruff^{c)}
Lawrence Livermore National Laboratory, Mail Stop L-637, 7000 East Avenue,
Livermore, California 94550

(Received 28 October 2005; accepted 2 March 2006; published online 8 May 2006)

Higher electron temperature ($T_e > 350$ eV) and reduced electron thermal diffusivity ($\chi_e < 10$ m²/s) is achieved in the Sustained Spheromak Physics Experiment (SSPX) by increasing the discharge current= I_{gun} and gun bias flux= ψ_{gun} in a prescribed manner. The internal current and q =safety factor profile derived from equilibrium reconstruction as well as the measured magnetic fluctuation amplitude can be controlled by programming the ratio $\lambda_{\text{gun}} = \mu_0 I_{\text{gun}} / \psi_{\text{gun}}$. Varying λ_{gun} above and below the minimum energy eigenvalue= λ_{FC} of the flux conserver ($\nabla \times \vec{B} = \lambda_{\text{FC}} \vec{B}$) varies the q profile and produces the m/n =poloidal/toroidal magnetic fluctuation mode spectrum expected from mode-rational surfaces with $q=m/n$. The highest T_e is measured when the gun is driven with λ_{gun} slightly less than λ_{FC} , producing low fluctuation amplitudes ($<1\%$) and $1/2 < q < 2/3$. Transport analysis shows a reduction in χ_e as T_e increases, differing from Bohm or open field line transport models where χ_e increases with T_e . Detailed resistive magnetohydrodynamic simulations with the NIMROD code support the analysis of energy confinement in terms of the causal link with the q profile, magnetic fluctuations associated with low-order mode-rational surfaces, and the quality of magnetic surfaces. © 2006 American Institute of Physics. [DOI: 10.1063/1.2192469]

I. INTRODUCTION

Spheromaks¹ formed with a single pulse followed by free decay in a flux conserver with a magnetized gun initially relax close to a stable, minimum energy Taylor state² with a well-defined ratio of poloidal to toroidal current, but then suffer from internal kink (or resistive tearing) mode instabilities^{3–6} as the colder, more resistive edge causes the poloidal current to decay faster than the toroidal current causing a loss of toroidal magnetic field. This instability is often disruptive enough to rapidly terminate the plasma discharge and is consistent with the internal normalized current profile $\lambda = \mu_0 j / B$ and safety factor profile $q = d\psi/d\phi$ with ψ =toroidal flux, ϕ =poloidal flux. Flatter λ profiles are more stable. Peaked (or hollow) profiles can cause the q profile to span mode-resonant surfaces. In the free decay case, the loss of toroidal magnetic field causes a peaking in the λ profile at the magnetic axis leading q to span the $m/n=1/2$ surface.

During the formation pulse, the gun current flowing down the open magnetic field lines near the geometric axis and returning near the outer wall back to the gun is large ($\lambda_{\text{gun}} \sim 2\lambda_{\text{FC}}$). The $n=1$ dough-hook^{7–9} mode, a distortion of the central plasma column, is active generating toroidal current and forming the spheromak configuration. The $n=1$ fluctuation amplitude is large enough ($\delta B/B > 10\%$) to represent significant nonaxisymmetry, and open field lines limit plasma temperature.^{10,11} The q profile (as calculated for the mean-field axisymmetric $n=0$ component of the magnetic field) is hollow with a minimum close to 1, and looks much

like the profile of a sawtooth tokamak. The large amplitude of the mode, however, calls into question the application of flux surfaces and a safety factor at this time of the discharge and previous experiments⁸ have shown the $n=1$ distortion to be a central column mode and not an internal mode. After the formation pulse, gun current drops, and the mean-field q drops below 1 to a reverse-shear profile: q is peaked at the magnetic axis with a minimum near the outer edge, and diverges at the mean field separatrix. The fluctuation amplitude of the $n=1$ column mode is reduced ($\delta B/B < 1\%$), the flux surface quality improves, confinement improves, and ohmic heating raises T_e . The configuration is axisymmetric with low fluctuations. However, without continued edge drive, resistive dissipation in the colder edge region causes λ to sag at the edge and peak at the magnetic axis, lowering q at the edge to $1/2$ and then $1/3$. The plasma responds by relaxing towards minimum energy, converting toroidal current into poloidal current¹² through the $q=m/n=1/2$ and $1/3$ modes now driven by the peaked λ profile. Often, the $m/n=1/2$ mode is sufficient to cause disruptive termination of the configuration before higher-order $n=3,4$ modes are observed.

It is shown here that the driving edge current with $\lambda_{\text{gun}} < \lambda_{\text{FC}}$ for an extended period of time after formation sustains the poloidal current, suppresses the $m/n=1/2$ mode, and allows the system to decay on the timescale of the toroidal current flowing in the hotter and more conductive core, thus greatly increasing the plasma lifetime. Most significantly, the q profile can be controlled during the discharge by adjusting the initial flux configuration and programming the discharge current. It is possible in the Sustained Spheromak Physics Experiment (SSPX) to maintain the q profile between reso-

^{a)} Paper UI2 2, Bull. Am. Phys. Soc. **50**, 344 (2005).

^{b)} Invited speaker.

^{c)} Present address: University of Washington, Dept. of Aeronautics and Astronautics, Seattle, WA 98195. Electronic mail: mclean1@llnl.gov

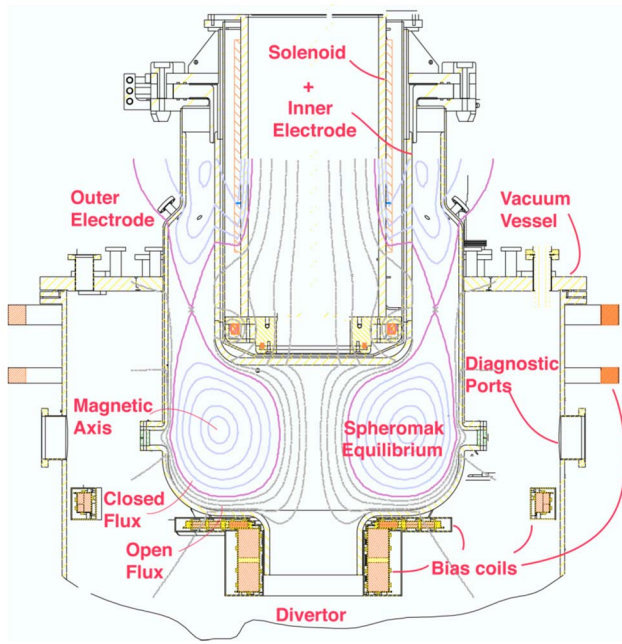


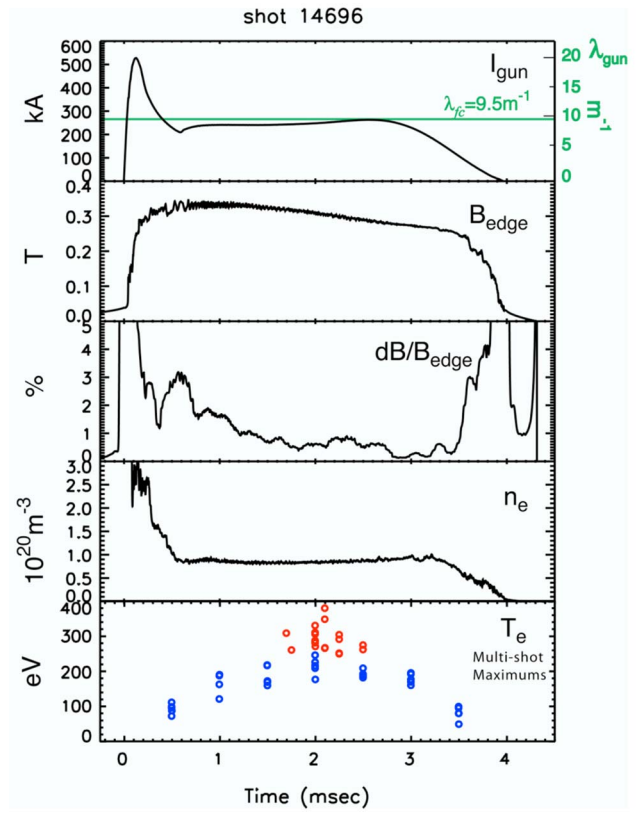
FIG. 1. (Color online) Side view of SSPX.

nant surfaces, precluding large global fluctuations for more than 2 ms (only limited by the available charge capacity of the sustainment capacitor bank), a much longer duration than previously¹³ achieved. We have identified that operating between the 2/3 and 1/2 modes produces the highest T_e in our configuration and produced the highest T_e (>350 eV) yet observed in a spheromak driven for these longer periods of time (several milliseconds).

II. RESULTS AND DISCUSSION

A. Description of SSPX geometry and operation

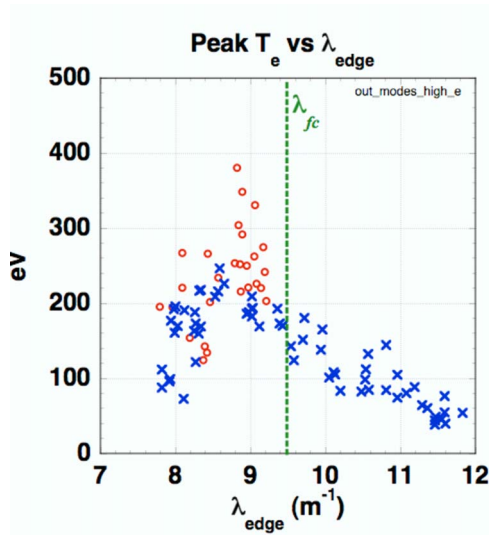
SSPX geometry is shown in Fig. 1. Time histories of several parameters are shown in Fig. 2. Other discharge parameters of interest are a toroidal current of ~ 500 kA, and a toroidal field at the magnetic axis of ~ 0.6 T. The time sequence for forming and sustaining a spheromak on SSPX is as follows: The external magnetic field bias coils are energized several seconds before a discharge to allow the bias magnetic flux to diffuse through the thick (20 mm) copper wall of the flux conserver. Fast-puff gas valves are fired ~ 250 μ s before discharge to allow gas to flow into the region between the electrodes. A formation capacitor bank (10 mF, 10 kV) is discharged, which ionizes the gas (hydrogen) and produces a large initial pulse of 500 kA [Fig. 2(a)]. A second, sustaining capacitor bank is then fired. This bank (120 mF, 5 kV) is arranged as a five-stage pulse-forming network to give a relatively constant flat-top current after formation. The large initial current pulse forms the spheromak as shown by the buildup of magnetic field to about 0.34 T at the outer midplane edge [Fig. 2(b)]. The gun current then drops and the flat-top current maintains the spheromak with edge magnetic fluctuations that evolve over time as shown in Fig. 2(c). The (chord-averaged) plasma electron density n_e [Fig. 2(d)] is high during formation, but falls to a

FIG. 2. (Color online) Discharge data for $T_e = 230$ eV shot.

constant level of 10^{20} m^{-3} until the end of the shot. To maintain density in this range, the vessel and flux conserver are gettered with titanium every five shots. Finally, the electron temperature is observed to increase to a peak value of ~ 350 eV, which then decreases until the end of the shot.

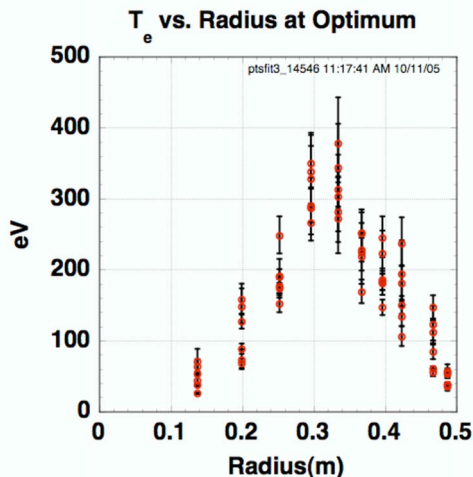
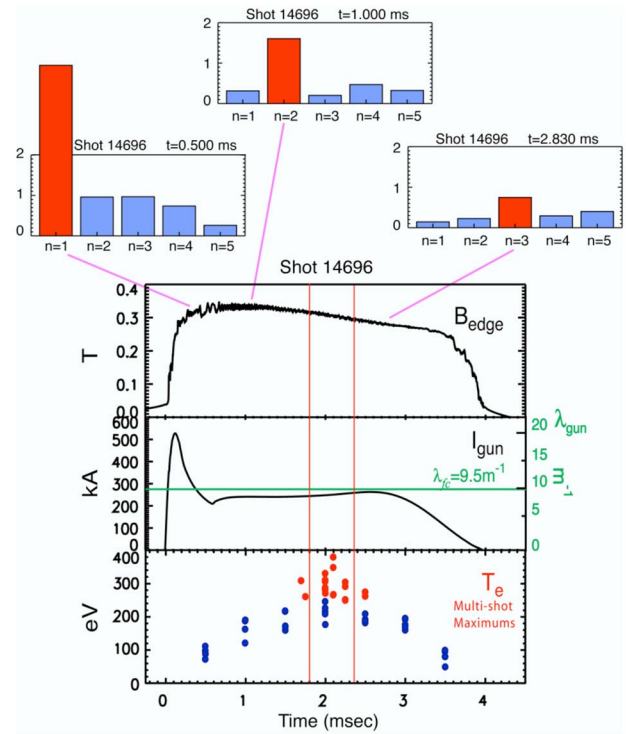
B. Optimum λ_{edge} produces the highest T_e

A series of shots were taken varying the bias magnetic flux in the gun from 20–30 mWb while holding the sustainment bank charge voltage constant (thus varying λ_{edge}) to determine the effect. The sustainment bank current varied slightly at constant charge voltage when changing the flux but was nominally 230 kA. This produced a variation in λ_{edge} ($6 \text{ m}^{-1} < \lambda_{\text{edge}} < 12 \text{ m}^{-1}$) above and below the eigenvalue of the flux conserver, $\lambda_{\text{FC}} = 9.5 \text{ m}^{-1}$. Thomson scattering measurements of T_e were taken 2 ms after breakdown, the expected peak in T_e . The results, plotted as blue \times 's in Fig. 3, clearly show an optimum λ_{edge} at about 9 m^{-1} , slightly less than λ_{FC} . Later, the sustainment bank charge voltage was raised to its rated maximum voltage and a few shots were taken. This produced a sustainment bank current of 260 kA. The flux was also raised to maintain λ_{edge} in the optimum range. These shots, shown as red circles in Fig. 3, resulted in the highest T_e yet observed on SSPX and close to the 400 eV observed on the compact toroid experiment (CTX) at the Los Alamos National Laboratory.^{23,24} Radial profiles of six high T_e shots are plotted in Fig. 4.

FIG. 3. (Color online) Highest T_e is observed with $\lambda_{\text{edge}} < \lambda_{\text{FC}}$.

C. Evolution of magnetic fluctuations during a discharge

Signals from an array of 14 Rogowski coils on the mid-plane posts are Fourier analyzed to determine the instantaneous amplitude and phase of toroidal spatial variations in the wall return current. The signals are decomposed into modes up to $n=5$. The analysis looks at signal frequencies of 1–100 kHz. The typical evolution of modes is shown in Fig. 5 along with the gun current and electron temperature measurements. A large amplitude $n=1$ is observed during the time the field is initially building, in agreement with observations on the SPHEX experiment⁹ and NIMROD modeling.¹⁴ After the formation current drops, an $n=2$ is observed followed by a relatively mode-free, quiescent period where the electron temperature reaches its highest value. Later, an $n=3$ often develops.

FIG. 4. (Color online) T_e profile at maximum available sustainment bank current and optimum λ_{edge} .FIG. 5. (Color online) Modes evolve from $n=1$ during formation to $n=2$ to a quiescent period to an $n=3$. Highest temperatures are observed during the quiescent period between the $n=2$ and $n=3$.

D. Equilibrium reconstructions show optimal λ_{edge} produces $1/2 < q < 2/3$

The mode evolution can be understood by considering the internal safety factor q profile from equilibrium reconstructions. For rational values of q , global magnetic fluctuations are expected with mode numbers $q=m/n$ =poloidal/toroidal mode numbers.

The CORSICA code¹⁵ reconstructs the internal field and currents by fitting the Grad-Shafranov equation to edge magnetic probes, gun current, and initial magnetic flux. Inside the separatrix, we use a parameterization of λ given by $\lambda = \lambda_0(1 + \alpha_4 \bar{\psi}^2)$; λ_0 is the value on the magnetic axis, $\bar{\psi} = (\psi - \psi_0)/(\psi_{\text{edge}} - \psi_0)$ is the normalized poloidal flux with ψ_0 , the value at the magnetic axis. The fitting parameter, α_4 , is positive for hollow profiles and negative when peaked. For current on the open flux outside the separatrix (λ_{edge}), studies of reconstructed profiles during the quiescent phase of the discharge find that $\lambda_{\text{edge}} = \text{const}$ provides the best fit to the magnetic probes.

A reconstruction of poloidal flux contours during the quiescent period (i.e., optimum λ_{edge}) is shown in Fig. 6 with a corresponding plot of λ , q , and T_e spatial profiles shown in Fig. 7. The equilibrium shows $1/2 < q < 2/3$ and a peaked λ profile, in agreement with the observations that mode amplitudes are low during this interval. Figure 7 shows that the peak in the T_e profile is aligned with the magnetic axis. Figure 8 overlays T_e vs ψ for T_e measured at a major radius $R > R_{\text{magnetic axis}}$ with T_e vs ψ for T_e measured at $R < R_{\text{magnetic axis}}$. These should overlay if the reconstructed

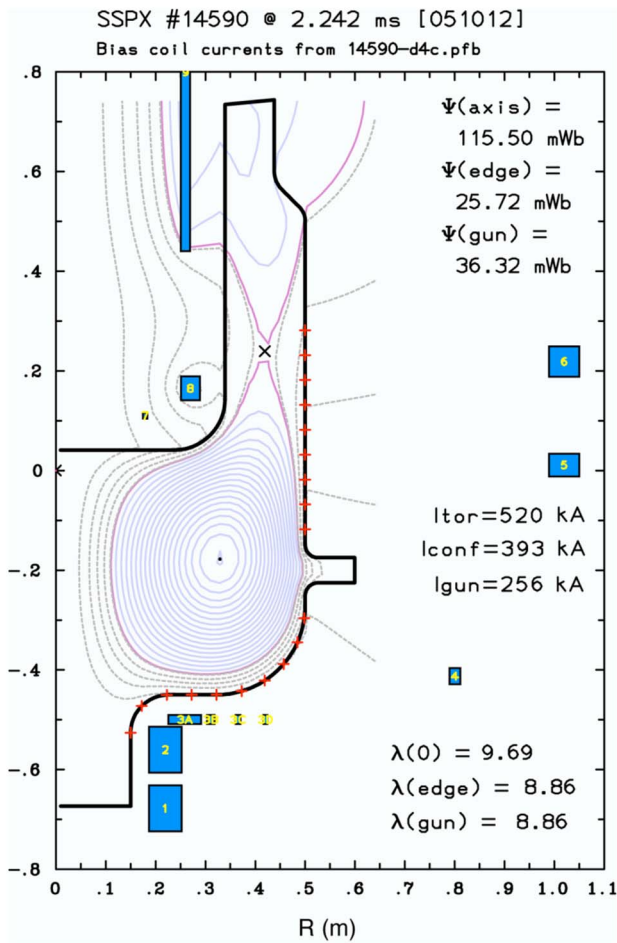


FIG. 6. (Color online) CORSICA equilibrium reconstruction showing flux contours and fitting parameters.

flux surfaces are isothermal, which indeed they do. This is good independent confirmation of the validity of the flux surface reconstruction.

E. Global fluctuations observed when λ_{edge} is not optimum

As λ_{edge} is varied from optimum, the q profile is varied and the expected magnetic fluctuating global modes are observed. Figure 9(a) shows a plot of safety factor q at the magnetic axis, q_0 , and the minimum in q near the separatrix, q_{min} , during a discharge along with amplitudes of the $n=2$ and $n=3$ toroidal modes. λ_{edge} varies with the discharge current, producing the change in q . When q_{min} drops below $1/2$, the amplitude of the $n=2$ mode increases and then drops out when q_{min} rises above $1/2$. The mode appears again near the end of the shot when the $q=1/2$ surface passes through the plasma again. Figure 9(b) shows a discharge where the q went too high and excited the $n=2/3$ mode.

CORSICA equilibrium reconstructions provide the relationship between q and λ for SSPX. This is plotted in Fig. 10(a). The $q=1/2$ and $q=2/3$ stability boundaries are identified and overlaid on the multishot temperature data in Fig. 10(b). T_e is consistently higher in the quiescent region and indicates that global magnetic fluctuations are a likely can-

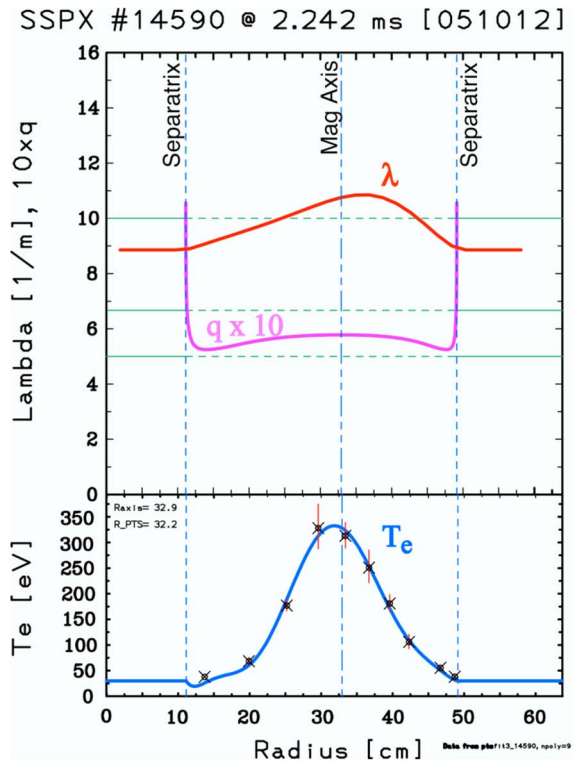


FIG. 7. (Color online) Internal λ and q profile (from equilibrium). T_e profile is peaked at the magnetic axis.

didate responsible for low T_e outside the optimum range of λ_{edge} . The mapping of these boundaries provides valuable guidance in operating the experiment.

An upgrade is in progress to double the sustainment bank energy and implement flexible, pulse-shaping, solid-state switching. This will allow for longer plasma discharges and more options for controlling the sustainment current during the discharge. This is expected to extend the quiescent interval from 2.5 to 8 ms.

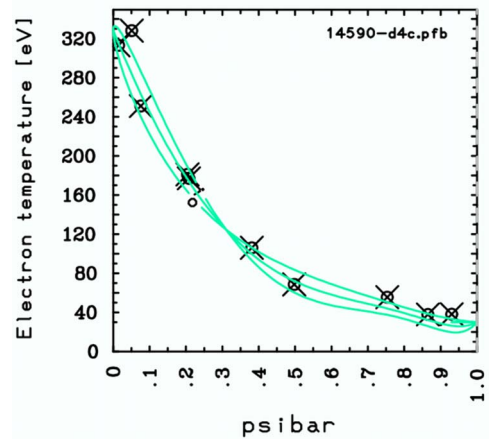


FIG. 8. (Color online) T_e aligns with reconstructed flux surfaces inboard and outboard of the magnetic axis.

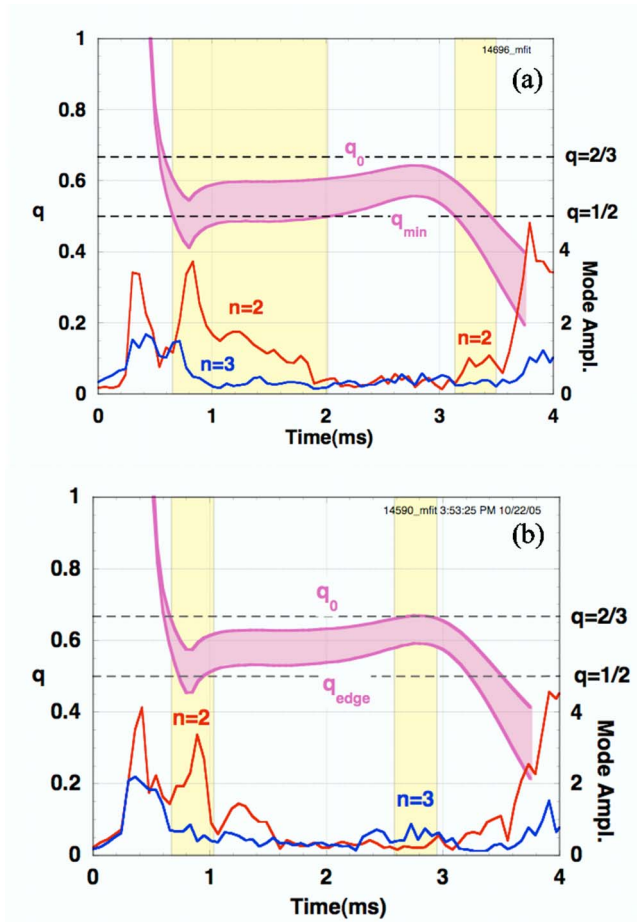


FIG. 9. (Color online) The expected modes are observed as the safety factor q spans different rational surfaces during the discharge. (a) The $n=2$ mode is excited at the beginning and end of the shot, reducing the duration of $n=2$, but getting high enough at the end to excite the $n=3$ mode. There is a narrow range of quiescent operation.

F. Transport profiles show good confinement in the core

Transport profiles show thermal diffusivity $\chi_e < 10 \text{ m}^2/\text{s}$ in the core of SSPX, approaching values measured in L-mode tokamak operation. The CORSICA code calculates the χ_e profile for each flux surface inside the separatrix by balancing heat flow out of each (mean-field) flux surface to the internal ohmic heating ($\eta_{sp} j^2$) within each flux surface:

$$\chi_e(\psi) = \frac{\int_0^\psi \eta_{sp} j^2 \left(\frac{d\text{vol}}{d\psi} \right) d\psi}{\text{Area}(\psi) \left(\frac{d\psi}{dr} \right) n_e k \frac{dT_e}{d\psi}}, \quad (1)$$

with k =Boltzmann's constant. Integration is taken from the magnetic axis out to each flux surface. T_e and n_e profiles are obtained by a polynomial fit of Thomson-scattering measurements onto equilibrium reconstructed flux surfaces. Off-axis peaking of the T_e profile can lead to negative values of χ_e in this calculation but, as shown in Fig. 8, T_e profiles for these shots are peaked on the magnetic axis and align well with flux surfaces both inboard and outboard of the magnetic axis.

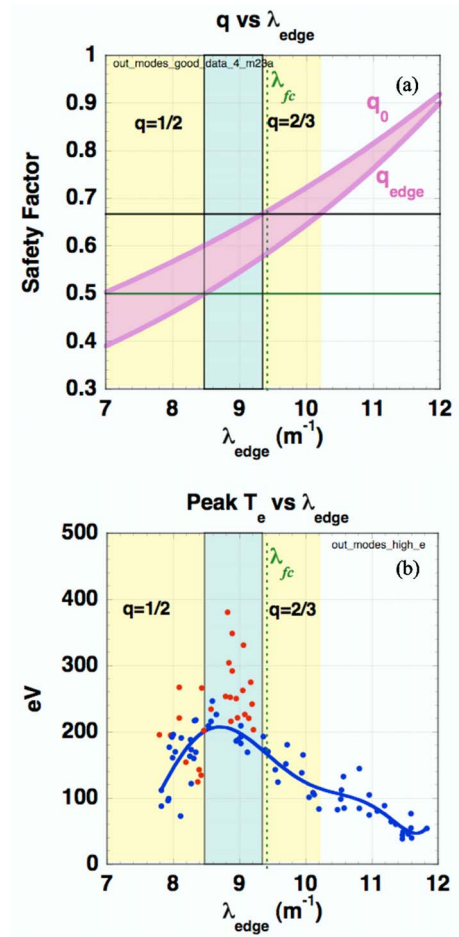


FIG. 10. (Color online) (a) Safety factor vs ledge showing stability boundaries for $m/n=1/2, 2/3$ modes. (b) Overlay of stability boundaries on the T_e data of Fig. 3 showing high T_e between the two unstable regions.

The calculation assumes steady state (data is taken at the peak in T_e versus time when $dT_e/dt \sim 0$), ohmic heating is the only electron heating source, ion-electron energy exchange is zero ($T_i=T_e$), no radiation heat loss ($P_{\text{rad}}=0$), and uses a temperature-dependent Spitzer resistivity η_{sp} with $Z_{\text{eff}}=2.3$. Profiles of T_e , ohmic heating density, and χ_e versus normalized radius are shown in Fig. 11. The difference between the T_e profiles for the various shots is representative of the shot-to-shot variation in T_e . Ohmic power is highest at the edge where T_e is lower and resistivity higher. For $r/a < 0.4$, however, the ohmic dissipation maintaining the high T_e is less than 10% of the total within the separatrix, indicating a good confinement in the core. The manner in which this relationship, that of good core confinement to a lossy edge, scales with size and perhaps other parameters will be important in determining the practicality of an eventual spheromak power reactor.

G. χ_e in the core near tokamak levels scales as $T_e^{-5/2}$

Scaling χ_e versus core T_e (Fig. 12) shows the regimes where various transport models may apply. A power law fit with $\chi_e \sim T_e^{-5/2}$ shows reasonable agreement with the data except at the highest values of T_e . Below 100 eV, fluctuation amplitudes are relatively high and fieldlines are expected to

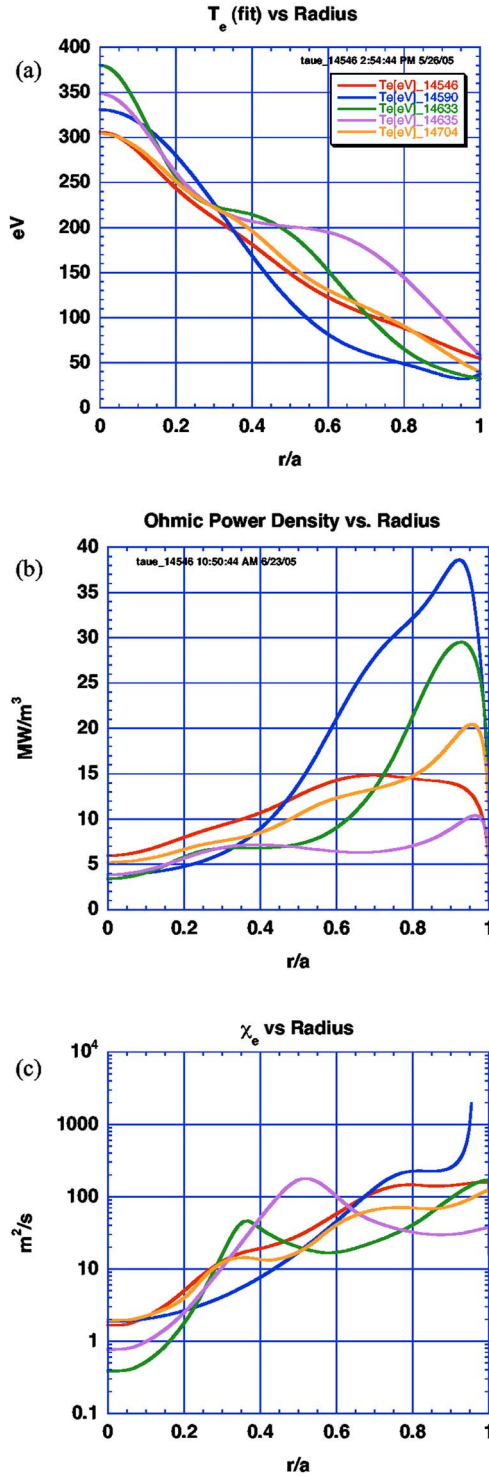


FIG. 11. (Color online) Transport properties of SSPX 350 eV shots (a), T_e (b) ohmic heating density, and (c) thermal diffusivity.

be stochastic. This curve is indicated by RR (for Rechester-Rosenbluth diffusivity), which in this regime can be given by¹⁶ $\chi_{RR} = v_{th} L_c (dB/B)^2$, where v_{th} is the electron thermal velocity, $L_c = [1/(v_{th} \tau_e) + 1/(2\pi R_{axis})]^{-1}$ is a correlation length taken to be the inverse sum of an electron mean free path length and one toroidal transit distance, and dB/B is the magnetic fluctuation amplitude in the radial direction. For

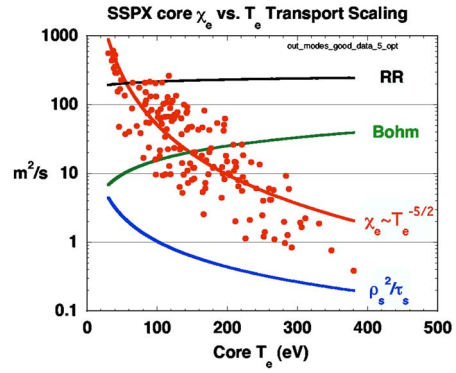


FIG. 12. (Color online) Scaling of χ_e vs T_e along with various transport models and power-law best fit through data showing $\chi_e \sim T_e^{-5/2}$.

scaling purposes here, we use the root mean square (rms) fluctuation of the poloidal field at the outer wall and assume this correlates with internal radial magnetic fluctuations. Magnetic fluctuations can be large in this temperature range driven by the previously described global fluctuations. Moving to higher T_e , values of Bohm diffusion given by $D_{Bohm} = T_e / 16B$ m²/s, T_e in eV, B in Tesla, give numbers in the range observed in SSPX. At the highest T_e , however, the thermal diffusivity is approaching the ion classical diffusivity given by $\chi_i = \rho_s^2 / \tau_s$, where ρ_s and τ_s are the ion Larmor radius and collision time calculated at T_e . This low value of calculated χ_e indicates the likelihood that the present analysis lacks important effects, particularly the contribution due to the ions. Hot ions have been observed consistently in spheromaks during formation and reconnection.¹⁷ Ion heating may play a large role in the initial heatup of the spheromak after formation.¹⁸ Conversely, the ions may also be cool due to charge exchange with background neutrals. Previous ion-Doppler spectrometry measurements of impurity ion temperatures on SSPX have shown $T_i > T_e$ soon after formation and $T_e \sim T_i$ during the quiescent phase but the uncertainties in these measurements have remained large due to low signal amplitudes. Improvements are needed and additional work is planned to study the ion channel, including new diagnostics (neutral particle analyzer for T_i measurements) and eventually neutral beam heating. The neutral beam heating system will be capable of delivering pulses of hot ions to study transient heating on the electrons from a population of hot ions. The upgrade to the sustainment bank system to extend the discharge time, discussed previously, will allow more time for initial formation transients to decay removing some of the uncertainty in the calculation of transport properties.

H. Three-dimensional modeling with NIMROD shows quantitative agreement

The NIMROD three-dimensional (3D), nonlinear, resistive magnetohydrodynamic (MHD) code¹⁹ has been used to simulate many aspects of spheromak physics.^{14,20–22} NIMROD simulations confirm the salient features of spheromak formation, showing how the growth of the $n=1$ central column mode driven by the current from the coaxial gun converts toroidal flux into poloidal flux and how the plasma relaxes

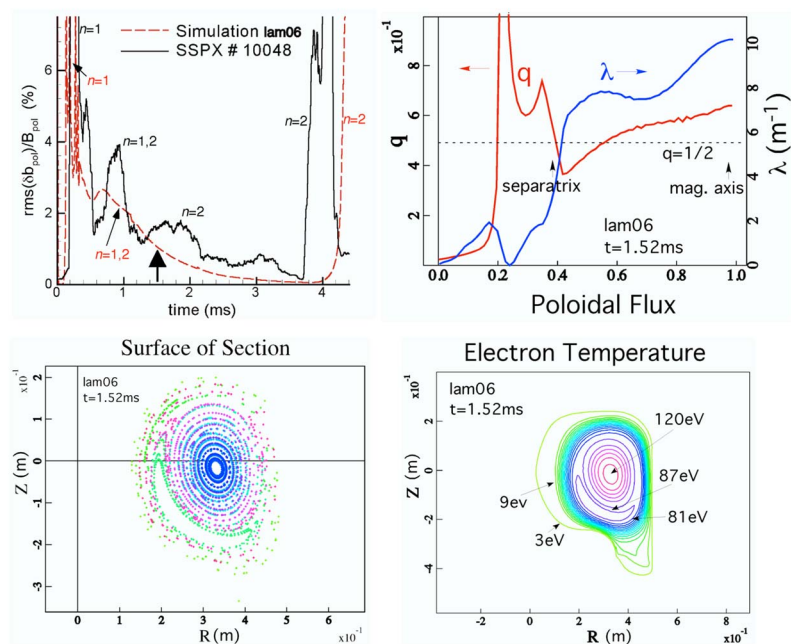


FIG. 13. (Color online) A comparison of NIMROD simulation and SSPX discharge magnetic perturbation time histories at the vertical midplane of the flux conserver just inside the radial boundary, q , and λ as functions of poloidal flux, a magnetic surface-of-section plot in the poloidal plane, and a poloidal contour plot of the electron temperature, all at $t=1.52$ ms.

when the current drive is reduced (partial sustainment) or decays allowing the symmetry-breaking magnetic perturbations to relax so that flux surfaces form and a hot plasma with a temperature profile that peaks on the magnetic axis can emerge.^{14,20–22} The NIMROD simulations agree relatively well with SSPX data, particularly with respect to the magnetics. Figure 13 shows a comparison of a NIMROD simulation and SSPX discharge magnetic perturbation time histories as measured in the vertical midplane of the flux conserver just inside the radial boundary. Figure 13 also shows q and λ as functions of poloidal flux, a magnetic surface-of-section plot in the poloidal plane, and a poloidal contour plot of the electron temperature at $t=1.52$ ms in the simulation at which time the relative magnetic perturbations are decreasing to $|\delta B/B| \leq 1\%$. The q profile indicates a $q=1/2$ surface just inside the separatrix, which correlates with an $m=1$, $n=2$ magnetic perturbation seen in the magnetic perturbation time history and in the surface-of-section and the electron temperature profile plots. However, most of the q profile in the closed flux region satisfies $1/2 \leq q \leq 3/5$, which promotes a significant volume of good magnetic surfaces and a peaked electron temperature profile (peak $T_e \sim 120$ eV in this simulation with $Z_{\text{eff}}=1$, described in Ref. 14). These and other NIMROD results support the perspective of this paper that the SSPX spheromak q profile is causally linked to the magnetic perturbations, which in turn influence the quality of the magnetic surfaces and the energy confinement.

III. SUMMARY

Globally coherent magnetic fluctuations are observed during the driven phase after spheromak formation in the SSPX by analysis of edge magnetic probe signals. The observed modes are low order, e.g., $m/n=q$ (safety factor) = poloidal/toroidal = $1/2$, $2/3$, and correlate with the internal

q profiles inferred by equilibrium reconstructions using the CORSICA code. The fluctuation mode numbers and amplitudes can be controlled significantly by programming the magnetic flux and the discharge current. Scanning the λ_{edge} above and below the minimum energy eigenvalue $= \lambda_{\text{FC}}$ of the flux conserver provides a variation in the internal q profile, producing the expected mode spectrum. By driving the edge with the proper λ_{edge} , the system can be operated with the mode spectrum between the $1/2$ and $2/3$ modes, producing low magnetic fluctuation amplitudes and high electron temperature $= T_e > 350$ eV. Since CORSICA does a good job predicting the mode spectrum, there is some confidence in the internal current profile generated by the code. Transport and confinement parameters calculated using Thomson scattering-measured T_e and n_e profiles coupled with the CORSICA current profile shows a reduction in electron thermal diffusivity as T_e increases. This scaling behavior is unlike Bohm or open field line transport models where thermal diffusivity increases with T_e . Detailed resistive MHD simulations with the NIMROD code support the analysis of SSPX energy confinement in terms of the causal link with the q profile, magnetic fluctuations associated with low-order mode-rational surfaces, and the quality of magnetic surfaces.

ACKNOWLEDGMENT

This work was performed under the auspices of the U.S. DOE by the University of California Lawrence Livermore National Laboratory under Contract No. W-7405-ENG-48.

¹M. N. Rosenbluth and M. N. Bussac, Nucl. Fusion **19**, 489 (1979).

²J. B. Taylor, Phys. Rev. Lett. **33**, 1139 (1974).

³A. Janos, G. W. Hart, C. H. Nam, and M. Yamada, Phys. Fluids **28**, 3667 (1985).

⁴S. O. Knox, C. W. Barnes, G. J. Marklin, T. R. Jarboe, I. Henins, H. W. Hoida, and B. L. Wright, Phys. Rev. Lett. **56**, 842 (1986).

⁵A. G. Sgro, A. A. Mirin, and G. Marklin, Phys. Fluids **30**, 3219 (1987).

⁶Y. Ono, R. A. Ellis, Jr., A. C. Janos, F. M. Levinton, R. M. Mayo, R. W.

- Motley, Y. Ueda, and M. Yamada, Phys. Rev. Lett. **61**, 2847 (1988).
- ⁷L. Lindberg and C. Jacobson, Astrophys. J. **133**, 1043 (1961)
- ⁸R. Duck, P. K. Browning, G. Cunningham, S. J. Gee, A. al-Karkhy, R. Martin, and M. G. Rusbridge, Plasma Phys. Controlled Fusion **39**, 715 (1997).
- ⁹P. K. Browning, G. Cunningham, S. J. Gee, K. J. Gibson, A. al-Karkhy, D. A. Kitson, R. Martin, and M. G. Rusbridge, Phys. Rev. Lett. **68**, 1718 (1992).
- ¹⁰E. B. Hooper, R. H. Cohen, and D. D. Ryutov, J. Nucl. Mater. **278**, 104 (2000).
- ¹¹R. Moses, R. A. Gerwin, and K. F. Shoenberg, Phys. Plasmas **8**, 4839 (2001).
- ¹²Y. Ono, M. Yamada, A. C. Janos, and F. M. Levinton, Phys. Fluids B **3**, 1452 (1991).
- ¹³H. S. McLean, S. Woodruff, E. B. Hooper, R. H. Bulmer, D. N. Hill, C. Holcomb, J. Moller, B. W. Stallard, R. D. Wood, and Z. Wang, Phys. Rev. Lett. **88**, 125004 (2002).
- ¹⁴B. I. Cohen, E. B. Hooper, R. H. Cohen, D. N. Hill, H. S. McLean, R. D. Wood, S. Woodruff, C. R. Sovinec, and G. A. Cone, Phys. Plasmas **12**, 056106 (2005).
- ¹⁵E. B. Hooper, L. D. Pearlstein, and R. H. Bulmer, Nucl. Fusion **39**, 863 (1999).
- ¹⁶A. B. Rechester and M. N. Rosenbluth, Phys. Rev. Lett. **40**, 38 (1978).
- ¹⁷J. C. Fernandez, C. W. Barnes, T. R. Jarboe, I. Henins, H. W. Hoida, P. L. Klingner, S. O. Knox, G. J. Marklin, and B. L. Wright, Nucl. Fusion **28**, 1555 (1988).
- ¹⁸K. J. Gibson, S. J. Gee, and M. G. Rusbridge, Plasma Phys. Controlled Fusion **37**, 31 (1995).
- ¹⁹C. R. Sovinec, A. H. Glasser, T. A. Gianakon, D. C. Barnes, R. A. Nebel, S. E. Kruger, D. D. Schnack, S. J. Plimpton, A. Tarditi, and M. S. Chu, J. Comput. Phys. **195**, 355 (2004).
- ²⁰C. R. Sovinec, J. M. Finn, and D. del-Castillo-Negrete, Phys. Plasmas **8**, 475 (2001).
- ²¹C. R. Sovinec, B. I. Cohen, G. A. Cone, E. B. Hooper, and H. S. McLean, Phys. Rev. Lett. **94**, 035003 (2005).
- ²²E. B. Hooper, T. A. Kopriva, B. I. Cohen, D. N. Hill, H. S. McLean, R. D. Wood, S. Woodruff, and C. R. Sovinec, Phys. Plasmas **12**, 092503 (2005).
- ²³T. R. Jarboe, I. Henins, A. R. Sherwood, C. W. Barnes, and H. W. Hoida, Phys. Rev. Lett. **51**, 39 (1983).
- ²⁴T. R. Jarboe, F. J. Wysocki, J. C. Fernandez, I. Henins, and G. J. Marklin, Phys. Fluids B **2**, 1342 (1990).